Flexural phonons and thermal transport in multilayer graphene and graphite

L. Lindsay, D. A. Broido, and Natalio Mingo

Flexural Phonons and Thermal Transport in Multi-Layer Graphene and Graphite

L. Lindsay,[1,2] D. A. Broido,[1] and Natalio Mingo[3,4]

[1]Department of Physics, Boston College, Chestnut Hill, MA 02467, USA

[2]Department of Physics, Computer Science, and Engineering, Christopher Newport University, Newport News, VA 23606, USA

[3]CEA-Grenoble, 17 Rue des Martyrs, Grenoble 38000, France

[4]Department of Electrical Engineering, University of California, Santa Cruz, USA

Abstract

We present a theory of the lattice thermal conductivity, κ_L, of multi-layer graphene (MLG) and graphite, which is based on an exact numerical solution of the Boltzmann equation for phonons. Dominant contributions to κ_L from out-of-plane or flexural phonons are found consistent with previous findings for single-layer graphene (SLG). However, the interaction between graphene layers in MLG and graphite breaks a selection rule on phonon-phonon scattering causing their κ_Ls to be much lower than that of SLG. C^{13} Isotopes are shown to be an important scattering mechanism, accounting for a ~15% additional drop in the κ_L of these systems. We demonstrate that κ_L converges to that of graphite after only ~5 layers, a consequence of the weak interlayer coupling. These findings are qualitatively consistent with recent measurements of κ_L for MLG.

Introduction – Graphene and graphite, along with other carbon based structures such as diamond and carbon nanotubes, have among the highest thermal conductivities of any known materials. In these systems, heat is carried by phonons, and around room temperature, the lattice thermal conductivity, κ_L, is limited by phonon-phonon interactions caused by the anharmonicity of the interatomic potential [1]. In diamond, the strong covalent bonding and light carbon atoms produce large phonon velocities and extremely restricted phase spaces for phonon-phonon scattering causing large amounts of heat to be transported by the two transverse acoustic (*TA*) and one longitudinal acoustic (*LA*) phonon branches[2, 3]. One might expect graphene to be the two-dimensional (*2D*) analogue to this with the majority of heat carried by one *TA* and one *LA* branch. However, along with these modes that vibrate in the plane of the graphene layer, there are also out-of plane vibrations—the so-called flexural modes. The lowest flexural phonon branch (labeled *ZA*) exhibits an unusual quadratic dispersion, $\omega \sim q^2$, making the group velocity vanish as $q \rightarrow 0$. As a result, it was natural to assume that the flexural modes carry little heat [4-8].

Recently, we have shown that exactly the opposite is true [9, 10]: The reflection symmetry about the graphene plane leads to a selection rule that strongly inhibits phonon-phonon scattering. This combined with their large thermal population causes *the ZA phonons to in fact provide the dominant contribution to κ_L, much more than the in-plane contributions combined*. This surprising result is consistent with recent thermal transport measurements on graphene structures [9, 11-13].

Graphene is the building block for graphite so it is natural to ask: 1) How are the magnitudes of $\kappa_{graphene}$ and $\kappa_{graphite}$ related? and 2) How does $\kappa_{graphene}$ evolve into $\kappa_{graphite}$ with increasing number of graphene layers? Experimentally, these questions have not been conclusively

answered yet. The measured room temperature values of κ_L for graphene are in the range $\kappa_{graphene} \sim 600\text{-}5800 \ Wm^{-1}K^{-1}$ [14-18] while $\kappa_{graphite} \approx 2000 \ Wm^{-1}K^{-1}$ [19]. Recent measurements of κ_L for multi-layer graphene (MLG) show that κ_L decreases with increasing layer number, N, but values for $N=4$ and $N\sim 8$ lie below that of $\kappa_{graphite}$ [20].

In this paper, we present a theory of thermal transport and κ_L for MLG and graphite in the context of our new picture of phonon transport where the flexural mode contributions dominate κ_L. We show that the interaction between graphene layers breaks the graphene selection rule on phonon-phonon scattering leading to a substantial reduction in the flexural mode contributions to κ_L, which in turn decreases monotonically with increasing number of graphene layers. This mandates that $\kappa_{graphene} > \kappa_{graphite}$. Furthermore, we find that with increasing layer number, the graphite limit is rapidly reached: κ_L evolves from $\kappa_{graphene}$ to $\kappa_{graphite}$ within only ~ 5 layers. These findings are in qualitative agreement with the recently measured trends for κ_L in MLG [20].

Interlayer Coupling—Layered graphene systems have strong in-plane covalent bonding of carbon atoms and weak Van der Waals coupling between planes. An optimized Tersoff empirical interatomic potential [21, 22] which gives improved fits to the acoustic phonon dispersions in graphite is used to describe the in-plane bonding. A Lennard-Jones potential is used for the interplanar bonding:

$$V_{LJ}(r_{ij}) = 4\varepsilon[(\sigma/r_{ij})^{12} - (\sigma/r_{ij})^{6}] \tag{1}$$

where the parameters ε and σ are adjusted to best fit the c-axis phonon dispersion for graphite [23] and r_{ij} is the distance between atoms i and j. The values: $\varepsilon=4.6$ meV and $\sigma=0.3276$nm gives a separation between carbon planes of $\delta=0.335$nm in agreement with the measured value [19]. We include only coupling between adjacent carbon planes.

The phonon dispersions for *N*-layered graphene (graphite) are calculated by diagonalizing the dynamical matrices:

$$D_{\alpha\beta}^{\kappa\kappa'}(\mathbf{q}) = \frac{1}{M}\sum_{l'}\Phi_{\alpha\beta}(0\kappa,l'\kappa')e^{i\mathbf{q}\cdot\mathbf{R}_{l'}} \qquad (2)$$

to obtain the phonon frequencies, ω_{λ}, for each two dimensional (three dimensional) wavevector, $\mathbf{q}$, on a grid throughout the Brillouin zone, where $\lambda = (\mathbf{q}, j)$ and j labels the phonon branch. In Eq. 2, $l\kappa$ esignates the κth atom in the lth unit cell whose lattice vector is $\mathbf{R}_l$, M is the mass of the Carbon atoms, and α and β are Cartesian components. Also in Eq. 2, $\Phi_{\alpha\beta}(0\kappa,l'\kappa')$ are second-order interatomic force constants which are determined by the combined Tersoff and Lennard-Jones potentials. For *N*-layer graphene, the phonon frequencies at each two-dimensional 2D $\mathbf{q}$ point considered are obtained by numerically diagonalizing the *6N×6N* dynamical matrix using a standard LAPACK routine for Hermitian matrices. For graphite, a corresponding *12×12* dynamical matrix is diagnonalized using the same routine for each 3D $\mathbf{q}$ point considered.

Our focus will be on the low frequency part of the phonon spectrum, a portion of which is shown in Fig. 1, since these branches carry most of the heat, and only in this range is the phonon dispersion different from graphene. *N*-layered graphene and graphite each have three acoustic branches with phonon frequencies $\omega_{\lambda} \to 0$ as phonon wave vector $\mathbf{q} \to 0$. In-plane transverse and longitudinal branches (TA_1 and LA_1) have linear dispersion near the Brillouin zone center while an out-of-plane, flexural branch (ZA_1) has quadratic dispersion, except for very small q [24, 25]. For the multi-layers (N>1), the weak interlayer coupling produces *N*-1 low-lying optic phonon branches for each acoustic branch, which we label $TA_{i>1}$, $LA_{i>1}$, and $ZA_{i>1}$. Note that the $TA_{i>1}$ and $LA_{i>1}$ branches deviate from TA_1 and LA_1 only very near the Γ-point, while the

flexural branches, $ZA_{i>1}$, deviate significantly from the ZA_1 branch throughout much of the Brillouin zone.

Breaking of Selection Rule–The intrinsic resistance to heat flow in graphene-based structures is limited by three-phonon scattering, which dominates κ_L around and above room temperature [1]. The phase space for this scattering is defined from all three-phonon processes satisfying the conservation of energy and momentum: $\omega_j(\mathbf{q}) \pm \omega_{j'}(\mathbf{q'}) = \omega_{j''}(\mathbf{q''})$ and $\mathbf{q} \pm \mathbf{q'} = \mathbf{q''} + \mathbf{K}$, where $\mathbf{K}$ is a reciprocal lattice vector, which is zero for normal processes and non-zero for umklapp processes. The strength of a three-phonon scattering process is governed by the matrix elements [10]:

$$\Phi_{\lambda\lambda'\lambda''} = \sum_{\kappa}\sum_{l'\kappa'}\sum_{l''\kappa''}\sum_{\alpha\beta\gamma}\Phi_{\alpha\beta\gamma}(0\kappa, l'\kappa', l''\kappa'')e^{\lambda}_{\alpha\kappa}e^{\lambda'}_{\beta\kappa'}e^{\lambda''}_{\gamma\kappa''}e^{i\mathbf{q'}\cdot\mathbf{R}_{l'}}e^{i\mathbf{q''}\cdot\mathbf{R}_{l''}} \tag{3}$$

The $\Phi_{\alpha\beta\gamma}(0\kappa, l'\kappa', l''\kappa'')$ are third-order anharmonic interatomic force constants (IFCs), and the $e^{\lambda}_{\alpha\kappa}$ are phonon eigenvectors. We have shown previously [9, 10] that reflection symmetry about a single graphene sheet (or any *2D* crystal) requires that the nth order anharmonic IFCs vanish: $\Phi_{\alpha_1...\alpha_n}(l_1\kappa_1;...;l_n\kappa_n) = 0$, when the number of out-of-plane components in the string, $\alpha_1...\alpha_n$, is odd. This leads to a selection rule that forbids any *n*-phonon scattering process involving an odd number of out-of-plane phonons. For the case of three-phonon scattering, the matrix element, Eq. 1, vanishes for processes such as *ZA+ZA↔ZA*, *ZA+TA↔LA*, *etc.* eliminating about 60% of the scattering phase space for *ZA* phonons and significantly increasing their intrinsic scattering times. This combined with their large thermal populations is why the *ZA* phonons provide the dominant contribution to κ_L in graphene.

In MLG and graphite, reflection symmetry applied to the nth order *interlayer* IFCs gives:

$$\Phi_{\alpha_1...\alpha_n}(l_1'\kappa_1';...l_i'\kappa_i';...;l_n'\kappa_n') = (-1)^m \Phi_{\alpha_1...\alpha_n}(l_1\kappa_1;...l_i\kappa_i...;l_n\kappa_n) \tag{4}$$

5

where *m* is the number of out-of-plane components in $\alpha_1 \ldots \alpha_n$ and $l_i'\kappa_i'$ designates the atom into which $l_i\kappa_i$ is mapped across the reflection plane (chosen to be in the middle of the structure). Since at least one of the $l_i\kappa_i$ resides in a different layer, Eq. 2 simply reduces the number of distinct IFCs but does not require any to vanish. As a result, the graphene selection rule does not hold, and the previously forbidden scattering becomes allowed providing additional resistance to phonon flow.

Thermal Transport Theory – We calculate κ_L for *N*-layer graphene and graphite using an exact numerical solution to the phonon Boltzmann transport equation (BTE), previously described elsewhere for single-walled carbon nanotubes (SWCNTs) [26, 27] and graphene [9, 10]. Solution of the BTE gives the non-equilibrium phonon distribution functions resulting from the temperature gradient applied across the graphene structure. These functions are directly related to τ_λ, the phonon lifetimes in mode λ. Here, the BTE is cast in terms of a set of coupled equations for these τ_λ:

$$\tau_\lambda = \tau_\lambda^0 + \tau_\lambda^0 \Delta_\lambda \tag{5}$$

In Eq. 5,

$$\Delta_\lambda = \sum_{\lambda'\lambda''}^{(+)} \Gamma_{\lambda\lambda'\lambda''}^{(+)} (\xi_{\lambda\lambda''}\tau_{\lambda''} - \xi_{\lambda\lambda'}\tau_{\lambda'}) + \frac{1}{2}\sum_{\lambda'\lambda''}^{(-)} \Gamma_{\lambda\lambda'\lambda''}^{(-)} (\xi_{\lambda\lambda''}\tau_{\lambda''} + \xi_{\lambda\lambda'}\tau_{\lambda'}) \tag{6}$$

where $\xi_{\lambda\lambda'} = v_{\lambda'}\omega_{\lambda'}/v_\lambda\omega_\lambda$ with v_λ being the velocity component along the transport direction, and the sums are over the phase space of λ,λ′, and λ″ satisfying energy and momentum conservation conditions for three-phonon scattering mentioned before Eq. 3. The $\Gamma_{\lambda\lambda'\lambda''}^{(\pm)}$ are the intrinsic anharmonic scattering rates:

$$\Gamma_{\lambda\lambda'\lambda''}^{(\pm)} = \frac{\hbar\pi}{4M^3} \begin{Bmatrix} n_{\lambda'}^0 - n_{\lambda''}^0 \\ n_{\lambda'}^0 + n_{\lambda''}^0 + 1 \end{Bmatrix} \left| \Phi_{\lambda,\pm\lambda',-\lambda''}^{(\pm)} \right|^2 \delta(\omega_\lambda \pm \omega_{\lambda'} - \omega_{\lambda''}) \tag{7}$$

with n_λ^0 being the Bose factor and $-\lambda \Rightarrow (-\mathbf{q}, j)$. The τ_λ^0 in Eq. 5 are the lifetimes within the relaxation time approximation (RTA) solution the BTE:

$$1/\tau_\lambda^0 \equiv \sum_{(+)} \Gamma_{\lambda\lambda'\lambda''}^{(+)} + 1/2 \sum_{(-)} \Gamma_{\lambda\lambda'\lambda''}^{(-)} + 1/\tau_\lambda^{bs} \qquad (8)$$

τ_λ^0 is directly determined by the intrinsic anharmonic scattering rates, and by any other extrinsic scattering processes. In this work, we include boundary scattering of phonons along the transport direction taken to be of length L. The choice: $\tau_\lambda^{bs} = L/2|v_\lambda|$ gives the correct limiting values of the thermal conductivity in the ballistic ($L \to 0$) and diffusive ($L \to \infty$) limits [28].

The BTE, Eq. 5 is solved using an iterative scheme. To begin this process, a grid of points is defined throughout the Brillouin zone. For each λ, the phase space of λ', λ'' are found numerically using a root-finding algorithm, and the anharmonic scattering rates are calculated from Eq. 7. This allows determination of τ_λ^0 from Eq. 8. $\tau_\lambda^{(0)} = \tau_\lambda^0$ is used then in Eq. 6 for the zero$^{\text{th}}$ iteration. Plugging into Eq. 5 yields $\tau_\lambda^{(1)}$. The iteration scheme is continued until the calculated κ_L from Eq. 9 (see below) differs negligibly on successive iterations. For MLG, the graphene BTE solution [9, 10] is generalized to include interlayer coupling, unit cell size of *2N*. For graphite, the unit cell contains 4 atoms and, *3D* $\mathbf{q}$-space must be used. Our approach automatically includes normal as well as umklapp processes. This is particularly important for graphene-based systems where the quadratic *ZA* dispersion makes normal scattering of low frequency phonons far more prevalent than is the case for systems having only linear acoustic branches [10].

The BTE solution yields the non-equilibrium distribution functions from which the phonon scattering times, τ_λ, are obtained. The κ_L for each system is determined from:

$$\kappa_L = \begin{cases} \dfrac{1}{(2\pi)^2(N\delta)} \sum_j \int (\partial n_\lambda^0/\partial T) \hbar \omega_\lambda v_\lambda^2 \tau_\lambda d\mathbf{q} & N-layer\ graphene \\[3ex] \dfrac{1}{(2\pi)^3} \sum_j \int (\partial n_\lambda^0/\partial T) \hbar \omega_\lambda v_\lambda^2 \tau_\lambda d\mathbf{q} & graphite \end{cases} \tag{9}$$

In the upper (lower) expression the integral is *2D* (*3D*).

Results and Discussion – In all calculations the thermal transport is along the $\Gamma \rightarrow M$ direction, and the lateral dimension has been taken to be infinite [29]. The breaking of the graphene selection rule for the multi-layers causes the phase space for three-phonon scattering to become very large and to increase rapidly with *N*. This presents a significant numerical challenge that has limited our consideration to $N \leq 5$. Figure 2 shows κ_L .vs. *N* (black circles) scaled by the calculated value: $\kappa_{graphene} \approx 3500 \mathrm{Wm^{-1}K^{-1}}$ for sample length, *L*=10μm, at temperature, *T*=300K (the typical sample lengths have L~1-10μm [14-16, 18, 20]). Also shown are the scaled per branch-type contributions to the total κ_L for each system, κ_{ZA}, κ_{TA}, and κ_{LA} (red, green, and blue circles), where $\kappa_{ZA} = \sum_{i=1}^{N} \kappa_{ZA_i}$, etc.. The contribution from high-lying optic branches is small and not shown. For graphite, the enormous three-phonon phase space has precluded a fully convergent result. Nevertheless, from the trend values obtained from the BTE solution for increasingly fine **q**-point grids, we have obtained an approximate thermal conductivity, $\kappa_{graphite}$, which we estimate to be within ~10% of the converged value (dashed black line). The dashed red, green, and blue lines correspond to the per branch-type values in graphite.

Over the full range of *N*, the *ZA* contribution is far larger than that from *TA* or *LA*: The thermal transport is dominated by the low-frequency out-of-plane ZA_i phonons, consistent with our previous findings for graphene [9, 10] and large-diameter SWCNTs [27]. Furthermore, κ_{TA} and κ_{LA} hardly vary with *N*, while κ_{ZA} decreases by almost 50% in going from *N=1* to *N=5*. The

substantial reduction of κ_L for MLG occurs in part because of the raised frequencies of the $ZA_{i>1}$ phonon modes and the stiffening of the low frequency ZA dispersion [24, 25]. However, *the primary reason for the drop in κ_L is the breaking of the graphene selection rule*. To demonstrate this, we note that $\kappa_{bilayer} = 0.73\kappa_{graphene}$ [30]. Recalculating $\kappa_{bilayer}$ with all three-phonon processes that violate the graphene selection rule artificially removed increases the ratio to $\kappa_{bilayer} = 0.92\kappa_{graphene}$. This shows that the selection rule violation accounts for ~70% of the drop in κ_L.

About 80% of the total decrease in κ_L occurs in going from graphene to the bilayer. By $N=5$ κ_L has essentially saturated to ~65% of $\kappa_{graphene}$ (κ_L drops by only 2% in going from $N=4$ to $N=5$). Thus, κ_L evolves from graphene to graphite within the first ~5 layers. The black dotted curve is a guide to the eye that highlights this behavior. This rapid transition occurs because the interlayer interactions are weak and short ranged causing a given graphene layer to only feel adjacent layers.

Figure 3 shows κ_L for $N=1$, *2* and *4* as a function of L in the range $L=1$-10μm. For small L, transport is ballistic and κ_L is independent of N. The observed stronger L dependence for graphene arises from the large intrinsic scattering times, τ_λ, for many ZA phonons, which allows them to travel ballistically across the sample. This is a consequence of the graphene selection rule. The *TA* and *LA* phonon contributions (not shown) have little L dependence over this range [10] reflective of diffusive transport arising from their smaller τ_λ. For MLG, the L dependence of κ_L becomes noticeably weaker because the breaking of the graphene selection rule provides new scattering channels for ZA phonons, which gives them a more diffusive behavior.

In real graphene and graphite samples, phonon scattering by isotopic impurities lowers κ_L. Similar to the derivation for cubic crystals [31], one can show that the graphene isotopic impurity scattering rates are: $1/\tau_F^{iso}(\omega) = gS_0\omega^2 D_F(\omega)$ and $1/\tau_{in}^{iso}(\omega) = gS_0\omega^2 D_{in}(\omega)/2$ where g is the mass

variance parameter (for carbon crystals, $g = 7.54 \times 10^{-5}$ for 1.1% C^{13} impurities in C^{12} [2]), S_0 is the area per carbon atom, and $D_F(\omega)$ and $D_{in}(\omega)$ are the densities of states per unit area for flexural (F) and in-plane (in) phonons. Using these expressions, we find a 10~15% reduction in the graphene and MLG κ_L shown in Figs. 2 and 3.

Our calculated κ_L for graphene is in reasonable agreement with measured values. Including the isotope scattering, we find $\kappa_L \approx 2600$ Wm^{-1}K^{-1} for L=5µm, which is just below the range of measured values for similar length samples from Refs. 14 and 15 (~3000-5800 Wm^{-1}K^{-1}), and within the range found in Refs. 16 and 18 (~1500-3500 Wm^{-1}K^{-1}). Large uncertainties [18] have thus far precluded experimental identification of a length dependence such as indicated in Fig 3. For MLG a large decrease in κ_L is observed with increasing number of layers [20]. This is qualitatively consistent with our theory, which predicts that the large drop comes from suppression of flexural phonon contributions. Conceptually, the out-of-plane vibrations should be more strongly affected by interlayer interactions than the in-plane modes since the latter's vibrations are parallel to the layers. Finally, our finding that κ_L saturates to the graphite value after only ~5 layers is qualitatively consistent with the measured saturation of ~8 layers [20].

Summary and Conclusions –A theory of κ_L in MLG and graphite has been developed, which highlights the dominant contributions of the flexural phonons. We have shown that the interlayer coupling breaks the graphene selection rule leading to a strong suppression of the flexural phonon contributions to κ_L and correspondingly large reductions in κ_L itself, establishing that $\kappa_{graphene} > \kappa_{graphite}$. The κ_L decreases monotonically with increasing number of layers and lies significantly below the graphene κ_L. Finally, κ_L converges to the graphite value after only ~5 layers reflecting the very limited range of the interlayer interactions. These findings are in reasonable agreement with a number of recent experiments on single and multi-layer graphene.

References

[1] J. M. Ziman, *Electrons and Phonons* (Oxford University Press, London, 1960).

[2] D. G. Onn, A. Witek, Y. Z. Qiu, T. R. Anthony and W. F. Banholzer, *Phys. Rev. Lett.* **68**, 2806 (1992).

[3] A. Ward, D. A. Broido, D. A. Stewart and G. Deinzer, *Physical Review B* **80**, 125203 (2009).

[4] P. G. Klemens, *J. Wide Bandgap Mater*. **7**, 332 (2000).

[5] P. G. Klemens, *Int. J. Thermophys.* **22**, 265 (2001).

[6] D.L. Nika, S. Ghosh, E.P. Pokatilov, and A.A. Balandin, *Appl. Phys. Lett.* **94**, 203103 (2009).

[7] D.L. Nika, E.P. Pokatilov, A.S. Askerov, and A.A. Balandin, *Phys. Rev. B* **79**, 155413 (2009).

[8] B. D. Kong, S. Paul, M. B. Nardelli and K. W. Kim, *Phys. Rev. B* **80**, 033406 (2009).

[9] J. H. Seol, I. Jo, A. L. Moore, L. Lindsay, Z. H. Aitken, M. T. Pettes, X. Li, Z. Yao, R. Huang, D. A. Broido, N. Mingo, R. S. Ruoff, L. Shi, *Science* **328**, 213 (2010).

[10] L. Lindsay, D.A. Broido, and N. Mingo, *Phys. Rev. B* **82**, 115427 (2010).

[11] W. Jang, Z. Chen, W. Bao, C.N. Lau, and C. Dames, *Nano Lett.* **10**, 3909 (2010).

[12] Z. Wang, R. Xie, T. C. Bui, D. Liu, X. Ni, B. Li and J. T. L. Thong, *Nano Lett*. **11**, 113 (2011).

[13] M. T. Pettes, I. Jo, Z. Yao, and L. Shi, *Nano Lett.* **11**, 1195 (2011).

[14] A. A. Balandin, S. Ghosh, W. Bao, I. Calizo, D. Teweldebrhan, F. Miao, and C. N. Lau, *Nano Lett.* **8**, 902 (2008).

[15] S. Ghosh, I. Calizo, D. Teweldebrhan, E. P. Pokatilov, D. L. Nika, A. A. Balandin, W. Bao, F. Miao, and C. N. Lau, Appl. Phys. Lett. **92**, 151911 (2008).

[16] W. Cai, A. L. Moore, Y. Zhu, X. Li, S. Chen, Li Shi, and R. S. Ruoff, *Nano Lett.* **10**, 1645 (2010).

[17] G. Faugeras, B. Faugeras, M. Orlita, M. Potemski, R. R. Nair and A. K. Geim, *ACS Nano* **4**, 1889 (2010).

[18] S. Chen, A. L. Moore, W. Cai, J. W. Suk, J. An, C. Mishra, C. Amos, C. W. Magnuson, J. Kang, L. Shi and R. Ruoff, *ACS Nano* **5**, 321 (2011).

[19] G. A. Slack, *Phys. Rev.* **127**, 694 (1962).

[20] S. Ghosh, W. Bao, D.L. Nika, S. Subrina, E.P. Pokatilov, C.N. Lau, A.A. Balandin, *Nature Materials* **9**, 555 (2010).

[21] J. Tersoff, *Phys. Rev. Lett.* **61**, 2879 (1988).

[22] L. Lindsay and D. A. Broido, *Phys. Rev. B* **81**, 205441 (2010).

[23] R. Nicklow, N. Wakabayashi, and H. G. Smith, *Phys. Rev. B* **5**, 4951 (1972).

[24] For MLG we find $\omega_{ZA}(q \to 0) \sim q^x$ with $2 > x > 1$ and x decreasing as N increases from *2* to *5*. We confirm numerically that in graphite $\omega_{ZA}(q \to 0) \sim q$, as pointed out in Ref. 28.

[25] A. Castro Neto, http://arxiv.org/pdf/1004.3682.

[26] L. Lindsay, D. A. Broido and N. Mingo, *Physical Review B* **80**, 125407 (2009).

[27] L. Lindsay, D.A. Broido, and N. Mingo, *Phys. Rev. B* **82**, 161402(R) (2010).

[28] N. Mingo and D. A. Broido, *Nano Lett.* **5**, 1221 (2005).

[29] Inclusion of lateral boundary scattering has only a modest effect on κ_L. Analytical considerations indicate that such scattering in *2D* layers is weaker than in nanowires (Z.

Wang and N. Mingo, unpublished).

[30] This large drop contrasts with Ref. 8 which found $\kappa_{bilayer} \approx \kappa_{graphene}$. Ref. 8 did not use a full

BTE solution or consider the graphene selection rule.

[31] S. Tamura, *Phys. Rev. B* **27**, 858 (1983).

Figure Captions

Figure 1 A portion of the low frequency part of the phonon dispersion showing the TA_i, LA_i and ZA_i branches. Purple curves are for both *N=2* and *N=4*; green curves are for *N=3*.

Figure 2   Calculated κ_L for multi-layer graphene .vs. layer number, *N*, for *N=1* to 5 (black circles). Also shown are the per branch contributions for *ZA* (red triangles), *TA* (green squares) and *LA* (blue diamonds) branches. The corresponding calculated graphite values are shown by the horizontal lines.

Figure 3 Calculated κ_L for graphene (*N=1*, solid black curve), bilayer graphene (*N=2*, dashed red curve), and quadlayer (*N=4*, dotted blue curve) as a function of sample length *L* for *T=300K*. On this scale, the *N=3* and *N=5* curves cannot be distinguished from that for *N=4*.
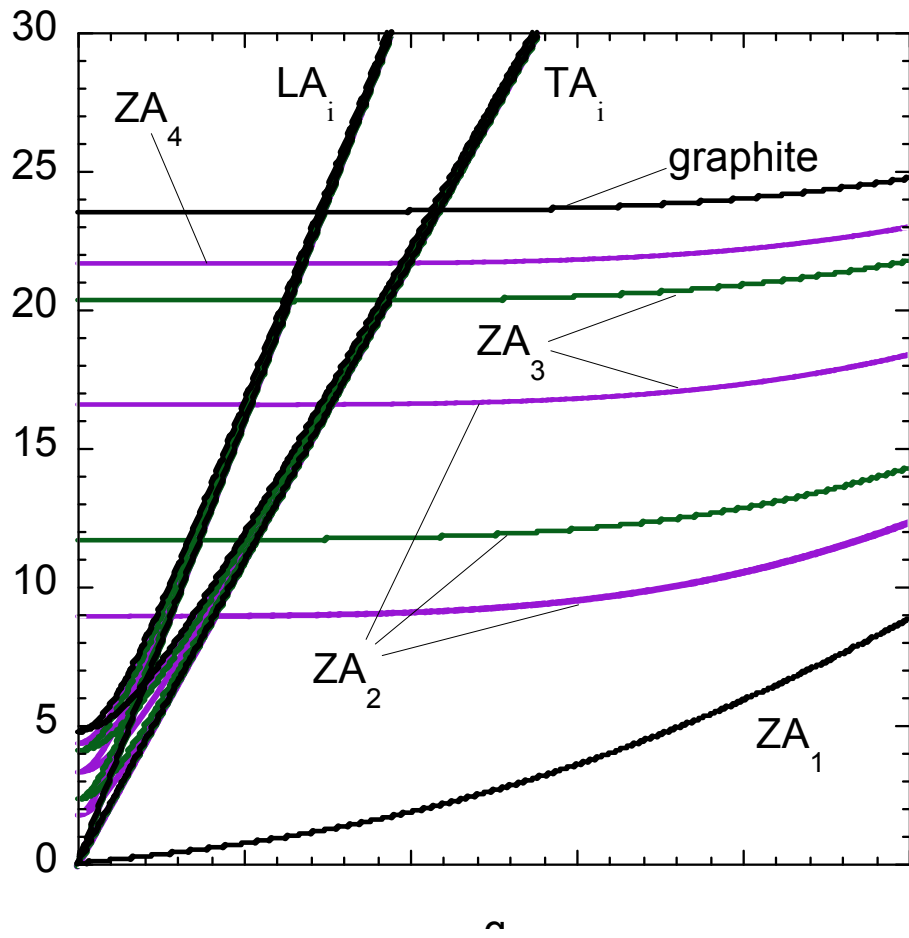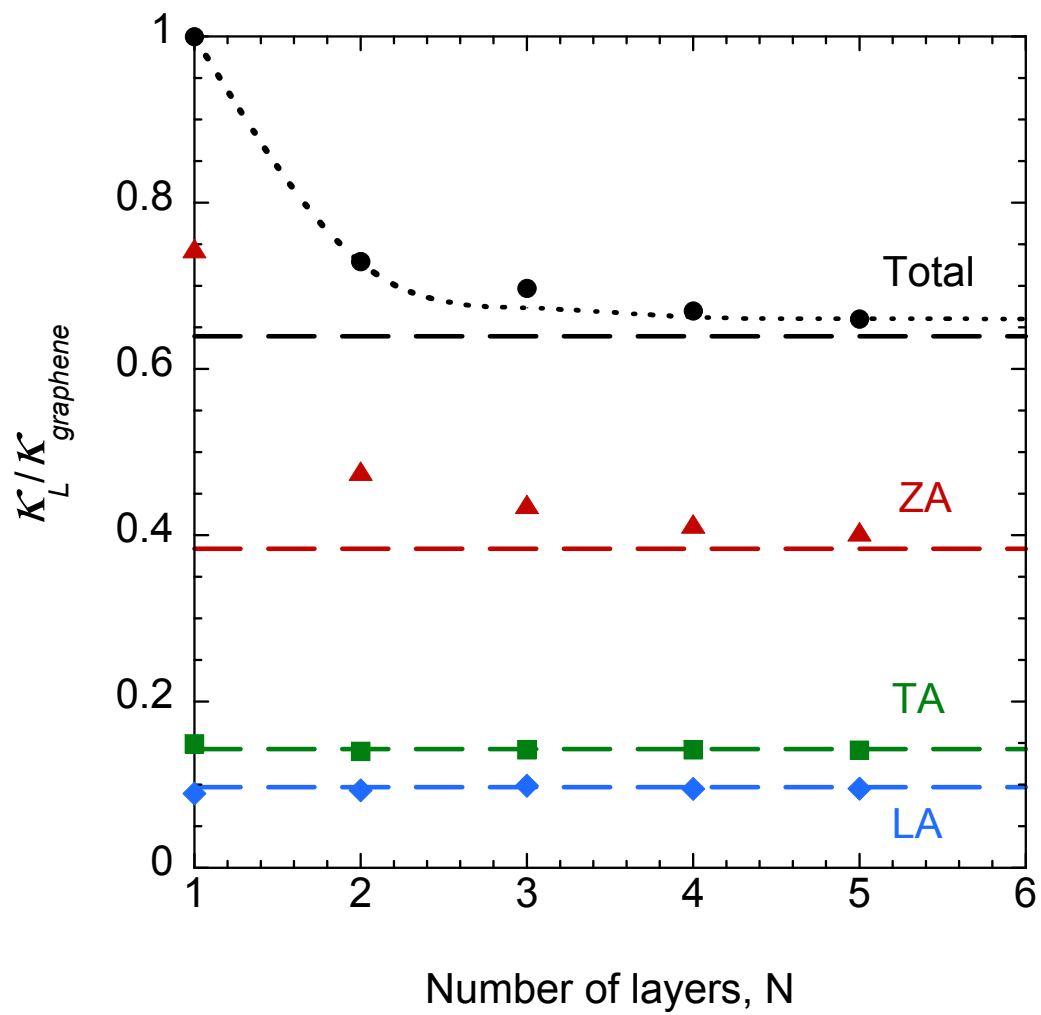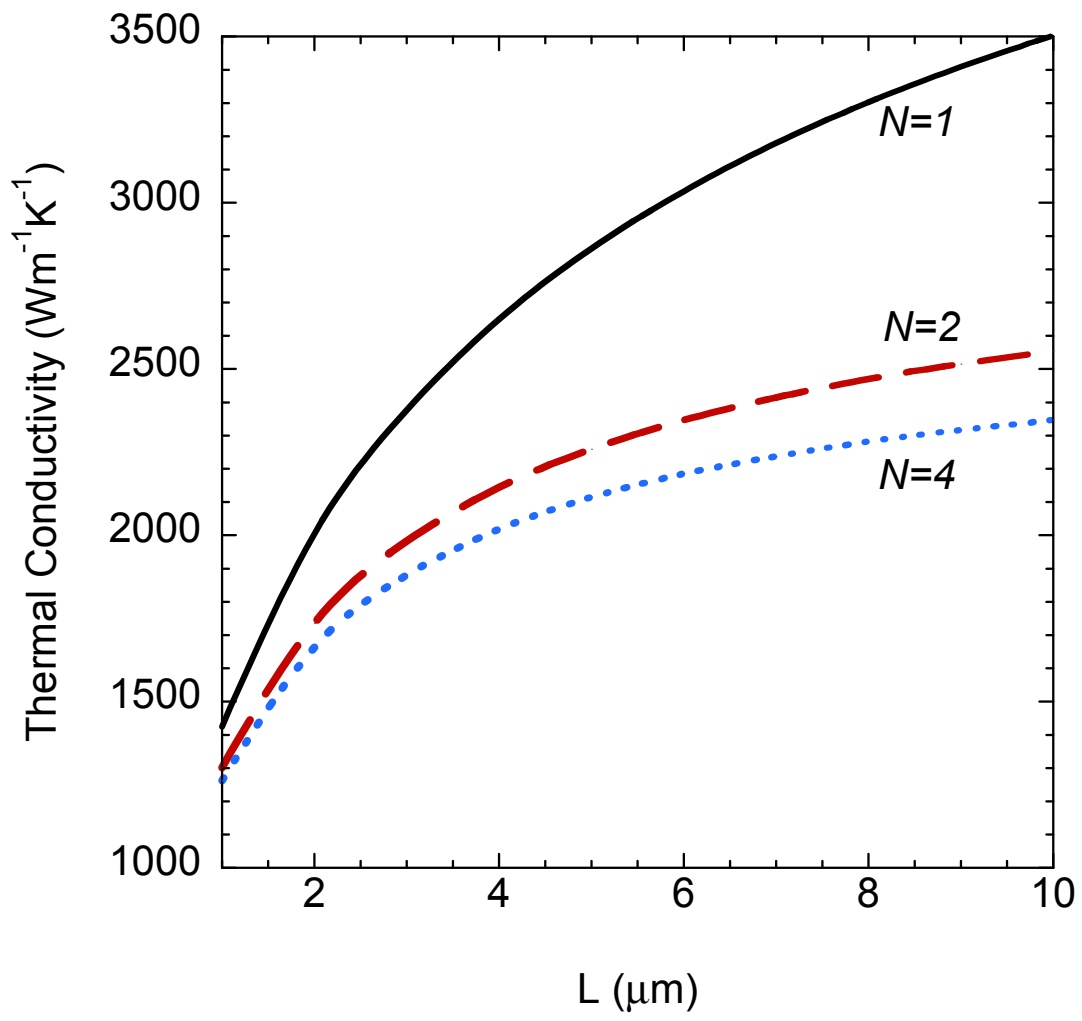
Figure 1

Figure 2

Figure 3